Ultrasound in Med. & Biol., Vol. 37, No. 6, pp. 958–970, 2011

0301-5629/$ - see front matter

ELSEVIER

doi:10.1016/j.ultrasmedbio.2011.02.017

● *Original Contribution*

CHARACTERIZING THE SUBHARMONIC RESPONSE OF PHOSPHOLIPID-COATED MICROBUBBLES FOR CAROTID IMAGING

Telli Faez,* Marcia Emmer,*† Margreet Docter,* Jeroen Sijl,‡ Michel Versluis,‡ and Nico de Jong*†‡

*Biomedical Engineering Thoraxcenter, Erasmus Medical Center, Rotterdam, The Netherlands; †Interuniversity Cardiology Institute of The Netherlands, Utrecht, The Netherlands; and ‡Physics of Fluids Group, Department of Science and Technology, University of Twente, Enschede, The Netherlands

(*Received* 18 *December* 2010; *revised* 22 *February* 2011; *in final form* 24 *February* 2011)

Abstract—The subharmonic vibration of BR14 (Bracco Research S.A., Geneva, Switzerland) contrast agent microbubbles is investigated within the preferable frequency range for carotid ultrasound imaging (8–12 MHz). The response of the bubbles was recorded optically with an ultra-fast recording camera (Brandaris 128) at three acoustic pressures (50, 100 and 120 kPa). The vibration of the microbubbles was measured as a function of the excitation frequency and its frequency content was determined. Among 390 recordings, 40% showed subharmonic oscillations. It was observed that for smaller microbubbles (diameter < 3 μm) the frequency of the maximum subharmonic response increases for increasing pressures (shell hardening) opposite to what has been reported for larger microbubbles (3 μm $<$ diameter $<$ 15 μm). These findings are well predicted by the model proposed by Marmottant et al. (2005) after including the dilatational shell viscosity of the microbubbles measured by Van der Meer et al. (2007), which indicates a marked shear-thinning behavior of the phospholipid shell. (E-mail: t.faez@erasmusmc.nl) © **2011 World Federation for Ultrasound in Medicine & Biology.**

Key Words: **Subharmonics, High frequency ultrasound, Ultrasound contrast agent, Microbubbles.**

INTRODUCTION

Clinical background

Atherosclerosis, a chronic, inflammatory disease involving the development of atherosclerotic lesions in the major arteries of the vasculature, is the uppermost underlying cause of cardiovascular disease (Yach et al. 2004) and a major cause of stroke (Golledge et al. 2000). Cardiac events and stroke are often caused by atherosclerotic plaque rupture. Plaques prone to rupture are called "vulnerable" (Virmani et al. 2000; Schaar et al. 2004). It has been shown that *vasa vasorum* plays an important role in atherosclerotic plaque pathogenesis and stability (Zamir et al. 1985; Barger et al. 1984). *Vasa vasorum* consists of a branching network of microvessels feeding the artery wall with nutrients and oxygen (Ritman et al. 2007; Gössl et al. 2003). Proliferation of the *vasa vasorum* into the plaque is suspected to lead to plaque growth and internal hemorrhage (Mause et al. 2009; Sluimer et al. 2009).

Ultrasound is an established tool to measure carotid atherosclerosis for the diagnosis and monitoring of patients at risk of stroke (Eliasziw et al. 1995; Baldassarre et al. 2000). The carotid artery is a relatively superficial artery that is easily accessible for ultrasound imaging. Recent advances in contrast-enhanced ultrasound have shown that this technique can characterize the carotid *vasa vasorum* and intra-plaque angiogenesis and, thus, it is potentially a new diagnostic tool to detect plaque vulnerability (Feinstein 2006; Shah et al. 2007; Vicenzini et al. 2007; Coli et al. 2008; Staub et al. 2009; Xiong et al. 2009; Shalhoub et al. 2010).

Contrast-enhanced ultrasound utilizes an ultrasound contrast agent containing gas-filled microbubbles. Due to their high compressibility, the microbubbles have a very high echogenicity in comparison with surrounding tissue (expressed as the contrast to tissue ratio, CTR). In the early days, only the linear vibration of the bubbles was utilized. The CTR can be further improved by exploiting the nonlinear properties of the contrast bubbles *e.g.*, in harmonic imaging: pulse inversion (Burns et al. 2000)

Address correspondence to: Telli Faez, Biomedical Engineering Thoraxcenter, Erasmus Medical Center, P.O. Box 2040, Dr. Molewaterplein 50, Office Ee 2032, 3000 CA Rotterdam, The Netherlands. E-mail: t.faez@erasmusmc.nl

and power modulation (Brock-Fisher et al. 1996). However, for the transmit pressures used in these methods (mechanical index (MI): 0.2–1.3), the CTR is lowered as a result of nonlinear propagation of the ultrasound wave through the tissue, which causes the tissue scattered signal to also contain energy at the second harmonic. Propagating ultrasound waves, however, do not contain energy at the subharmonic frequency, which revives a strong interest in subharmonic emissions (backscattered energy at half the transmit frequency) from contrast agents (Shi et al. 1999; Frinking et al. 2001; Chomas et al. 2002). Subharmonic imaging has potentially a larger CTR compared with other imaging methods (Shankar et al. 1998). In recent studies, the subharmonic response of Definity (Lantheus Medical Imaging, North Billerica, MA, USA) has been used to detect microvascularity in mice using an ultrasound biomicroscopy (UBM) system (Goertz et al. 2005) and in rabbit aortas using an intravascular ultrasound scanning system (IVUS) (Goertz et al. 2007; Needles et al. 2010).

Physical background

Several experimental (de Santis et al. 1967; Neppiras 1969) and theoretical (Eller 1969; Prosperetti 1975; Lauterborn 1976) studies have been performed to investigate and to describe the subharmonic resonance of bubbles. This nonlinear effect originates from a parametric instability in the equations describing the bubble dynamics (Plesset 1949). Prosperetti (1974) showed analytically that subharmonic oscillations occur for the amplitude of acoustic pressure above a certain threshold value. This threshold value was found to be minimal when the bubble oscillates at a frequency of twice its resonance frequency. It was also shown that damping increases the threshold pressure for the occurrence of subharmonic for free gas bubbles (Eller 1969; Prosperetti 1974, 1977).

Ultrasound contrast bubbles are coated to prolong their *in vivo* lifetime. The coating not only prevents a quick dissolution of the bubble gas but also has an increased shell viscous damping effect on the bubble oscillations in an ultrasound field. Since the viscoelastic shell of contrast agent microbubbles is known to increase the damping considerably (de Jong 1993; Van der Meer et al. 2007), it is expected that the subharmonic threshold pressure increases. This hypothesis was supported by Shankar et al. (1999). In that study, a purely viscoelastic shell model (de Jong et al. 1993; Church 1995; Hoff et al. 2000) was used to analyze the subharmonic behavior of coated bubbles. They confirmed the increase of the threshold pressure for the generation of the subharmonic by an increased damping. However, experimental studies on both albumin-coated (Optison, GE Healthcare, Chalfont St Giles, UK, and Albunex, Molecular Biosystems, San Diego, CA, USA) and phospholipid-coated (SonoVue, Bracco, Milan, Italy) contrast agents have shown that the threshold pressure to generate a subharmonic echo is lower than what was found for the uncoated bubbles (Chang et al. 1995; Lotsberg et al. 1996; Shankar et al. 1998, 1999; Krishna et al. 1999; Biagi et al. 2007; Frinking et al. 2010).

Recently, Frinking et al. (2009) and Sijl et al. (2010) have shown that the coating of lipid bubbles decreases the subharmonic threshold pressure. During buckling of the lipid coated shell, the bubbles show a highly nonlinear behavior at low acoustic pressures, such as asymmetric oscillation amplitudes whereby the compression amplitude outweighs expansion. This type of behavior is called "compression-only" behavior (de Jong et al. 2007). Marmottant et al. (2005) explained that this behavior is caused by a variable surface tension of lipid coated bubbles. Sijl et al. (2010) show that the initiation of subharmonic in phospholipid-coated microbubbles at lower threshold pressure can be explained with the Marmottant et al. (2005) model. They employ a weak nonlinear analysis of the Rayleigh-Plesset equation and, instead of using a pure elastic model, they describe the shell elasticity of coated bubble as an effective surface tension that varies strongly with the amplitude of oscillation, as proposed by Marmottant et al. (2005). Sijl et al. showed that this mechanism is responsible for the generation of subharmonic oscillations at low acoustic pressures. They report subharmonic threshold values down to 5 kPa for individual lipid-coated BR14 bubbles at driving frequencies between 1 and 4 MHz.

At present, studies on microbubbles subharmonic response have been performed at frequencies relevant for precordial imaging (1–4 MHz). However, the preferred ultrasound frequency for carotid imaging is between 5 and 15 MHz, involving microbubbles that are substantially smaller and may have different behavior. It is, however, unclear at what driving frequency the subharmonic response is maximal and how the response changes with varying driving pressure. The aim of this study is to investigate the dependence of the subharmonic response of a phospholipid-coated microbubble to the acoustic pressures applied at frequencies near 10 MHz.

For uncoated bubbles, it is well known that the fundamental resonance curve becomes asymmetrical and that the frequency of maximum response decreases with increasing acoustic pressure (Prosperetti 1975; Lauterborn 1976). Van der Meer et al. (2007) studied experimentally the fundamental resonance curve of phospholipid-coated microbubbles at constant acoustic pressure of 40 kPa and found an increase of the resonance frequency with respect to uncoated bubbles as a result of increased stiffness of the system. Later, Overvelde et al. (2010) investigated the fundamental resonance curves of the same microbubbles as a function of the acoustic

pressure. They observed a decrease in the resonance frequency of the microbubbles by increasing the amplitude of the acoustic pressure. Their results were in good agreement with the predictions of the Marmottant et al. model (2005). Yet, it is not known if the subharmonic response of a microbubble follows the same trend as its fundamental response. Furthermore, the radial dependence of shell viscosity characterized by Van der Meer et al. (2007) from the linearized bubble dynamics equations has not been implemented as of this time in the full context of the Marmottant et al. (2005) model (see for example Overvelde et al. 2010; Sijl et al. 2010).

In the present study, we investigate the subharmonic response of a microbubble around 10 MHz as a function of the acoustic pressure both numerically and experimentally. The influence of shell properties, effective surface tension and shell viscosity reported by Van der Meer et al. (2007), on the subharmonic response of phospholipid-coated microbubbles is determined in the simulations based on the Marmottant et al. (2005) model. The subharmonic responses of single bubbles are recorded optically using an ultra-high speed camera system. We apply microbubble spectroscopy as described by Van der Meer et al. (2007) by recording the subharmonic response of the bubbles at driving frequencies ranging from 4 to 7 MHz and from 8 to 12 MHz with a frequency step of 200 kHz leading to its subharmonic resonance curve. Bubble responses are measured at acoustic pressures of 50, 100, and 120 kPa. The experimental results are compared with bubble dynamics simulations based on the model of Marmottant et al. (2005).

THEORY AND MODELLING

Numerical model

To investigate the influence of the acoustic pressure and the driving frequency on the fundamental and subharmonic response of coated bubbles, we simulate the bubble dynamics with the model of Marmottant et al. (2005). The models describing the dynamics of coated microbubbles are an extension of the so-called Rayleigh-Plesset equation for free gas bubbles (Plesset and Prosperetti 1977) with the inclusion of shell viscosity and shell elasticity. The difference between this equation and that of a free gas bubble equation is the radius dependency of the effective surface tension and an additional dissipative term representing the viscosity of the shell. The Marmottant model has been shown to accurately simulate highly nonlinear behavior such as compression-only behavior and subharmonic oscillations, which is observed for individual bubbles using high-speed imaging (De Jong et al. 2007; Sijl et al. 2010).

The Rayleigh-Plesset-type equation used here is the following (Keller and Miksis 1980; Marmottant et al. 2005):

$$\rho\left(R\ddot{R}+\frac{3}{2}\dot{R}^2\right)=\left(P_0+\frac{2\sigma(R_0)}{R_0}\right)\left(\frac{R_0}{R}\right)^{3\kappa}\left(1-\frac{3\kappa}{c}\dot{R}\right) -P_0-\frac{2\sigma(R)}{R}-\frac{4\mu\dot{R}}{R}-\frac{4\kappa_s\dot{R}}{R^2}-P(t) \quad (1)$$

where R_0 and R are the initial and time-dependent radius of the bubble, ρ is the liquid density, μ is the dynamic viscosity of the liquid, c the speed of sound and κ the polytropic exponent of the gas inside the bubble. P_0 and $P(t)$ are the ambient and driving pressures, respectively. κ_s is the surface viscosity of the shell, which in the original equation is assumed to be independent of the initial bubble radius and $\sigma(R)$ is the effective surface tension. Three regimes are considered for a bubble shell in this model: buckled, elastic and ruptured. $\sigma(R)$ is defined as follows:

$$\sigma(R)=\begin{cases}0 & \text{If } R<R_b \text{ (buckled)}\\ \chi\left(\frac{R^2}{R_b^2}-1\right) & \text{If } R_b<R<R_r \text{ (elastic)}\\ \sigma_w & \text{If } R\geq R_r \text{ (ruptured)}\end{cases} \quad (2)$$

χ represents the shell elasticity. When the bubble is smaller than a defined buckling radius (R_b), the surface tension is zero and the elastic term vanishes. This state is called the buckled regime. The bubble is in the ruptured regime when its radius exceeds a certain radius (R_r) where the coating of the bubble breaks up and the gas inside the bubble is in direct contact with the surrounding liquid. In this case, the surface tension equals the surface tension of water (σ_w) and the elastic term is again zero. Between these two regimes, the shell coating is considered a purely elastic material.

From this model, we derive the resonance frequency of a coated microbubble. We assume small oscillation amplitudes and approximate the effective surface tension in the viscoelastic regime to its first-order Taylor expansion:

$$\sigma(R)=\sigma(R_0)+2\chi\left(\frac{R}{R_0}-1\right) \quad (3)$$

Combining eqn (3) with the linearization of eqn (1) yields the resonance frequency of a bubble with a linear viscoelastic shell:

$$f_{res}=\frac{1}{2\pi}\sqrt{\frac{1}{\rho R_0^2}\left[3\kappa P_0+\frac{2(3\kappa-1)\sigma(R_0)}{R_0}+\frac{4\chi}{R_0}\right]} \quad (4)$$

For $\chi = 0$ and $\sigma(R_0) = \sigma_w$, f_{res} represents the resonance frequency of an uncoated bubble, also known as the Minnaert frequency f_M (Minnaert 1933), including surface tension.

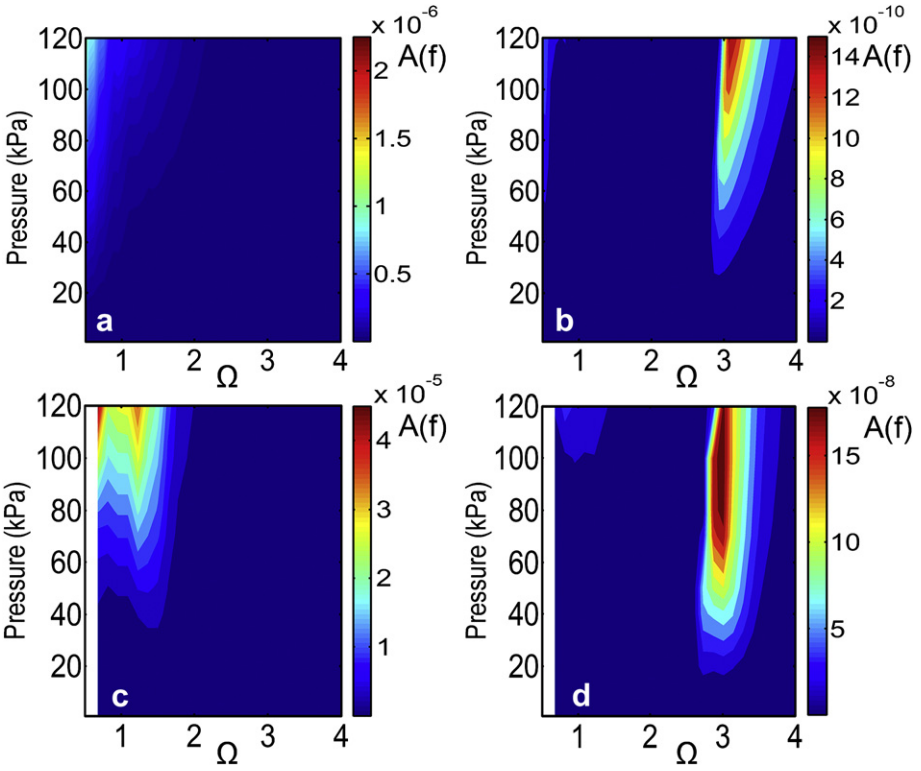

Fig. 1. Fundamental (left panel) and subharmonic (right panel) resonance curves of a 2 μm diameter coated bubble (a) and (b), and a 4 μm diameter coated bubble (c) and (d) vs. acoustic pressure amplitudes of 1–120 kPa. The normalized frequency *(Ω)* is defined as the driving frequency divided by the Minnaert frequency (Minnaert 1993) of an uncoated bubble. Shell parameters: $\sigma(R_0) = 0$, $\chi = 2.50$ N/m and $\kappa_s(R_0)$ taken from Van der Meer et al. (2007).

We used the Marmottant et al. (2005) model to simulate the fundamental and subharmonic responses of bubbles of different size (2 and 4 μm diameter), for increasing acoustic pressures (1–120 kPa). The pressure signal used in these simulations was a burst of 25 cycles tapered with a Gaussian envelope at the first and last two cycles.

To get subharmonic oscillations, a rapid change in the elasticity is required. In the elastic regime, the elasticity does not change or at least not very rapidly. Among the other two possible regimes, it has been observed (Sijl et al. 2010) that a bubble in the buckled state shows the highest amplitude of subharmonic response. Therefore, in the simulations, we choose the buckled state as the initial state of the bubble at its equilibrium position, $R = R_0$, *i.e.*, the initial surface tension is negligible and $\sigma(R_0) = 0$. $\sigma(R_0)$ reveals immediately the bubble's initial state, therefore, we derive R_b from $\sigma(R_0)$ *via* the following equation:

$$R_b = R_0 \Big/ \sqrt{\frac{\sigma(R_0)}{\chi} + 1} \tag{5}$$

instead of taking R_b as a constant as was done by Marmottant et al. (2005) (see also Overvelde et al. 2010). The other shell parameters were set as $\chi = 2.50$ N/m (Overvelde et al. 2010) and $\kappa_s(R_0)$ was considered dependent on the initial bubble radius using the measurements done by Van der Meer et al. (2007). The fundamental and subharmonic oscillation amplitudes of the bubbles were determined using the squared Fourier transform (FT) of the normalized radial excursion of the bubble.

$$A(f) = \left(FT\left[\frac{R(t)}{R_0}\right]\right)^2 \tag{6}$$

The results were plotted vs. the normalized frequency, Ω, which is defined as the driving frequency divided by the Minnaert frequency, f_M, (Minnaert, 1933) of an uncoated bubble. This leads to the fundamental and subharmonic resonance curves of the bubble.

Simulation results

Figure 1 shows the fundamental and subharmonic resonance curves of a 2 μm [(a) and (b)] and a 4 μm [(c) and (d)] diameter coated bubble as a function of the acoustic pressure (1–120 kPa). It can be seen that the coated bubble with 2 μm diameter indicates an over damped system in which no local maximum exists in

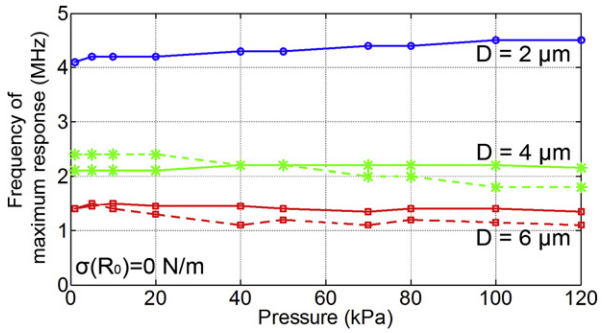

Fig. 2. Frequency of maximum response at the fundamental (driving) frequency (dashed lines) and the frequency of maximum response at the subharmonic frequency (solid lines) of different bubble sizes vs. applied acoustic pressures. Shell parameters: $\sigma(R_0) = 0$ N/m, $\chi = 2.50$ N/m, $\kappa_s(R_0)$.

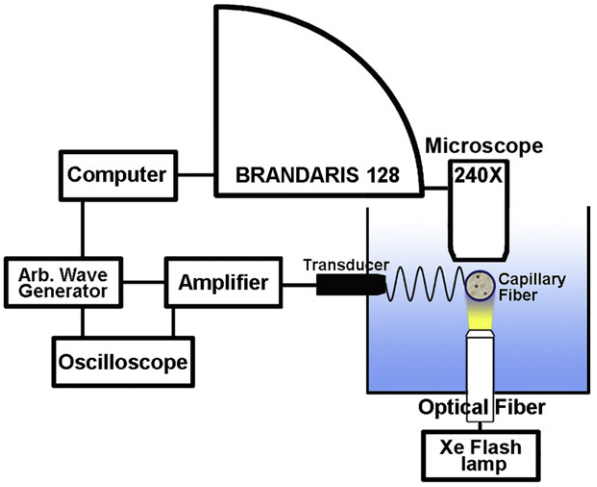

Fig. 3. Schematic view of the set up.

the radial oscillation amplitudes at the fundamental response of the bubble (Fig. 1a). Whereas for a 4 μm diameter bubble (Fig. 1c), the maximum fundamental response occurs when Ω is 1.30. For the subharmonic resonance curves, it is indicated that the maximum subharmonic amplitude for a coated bubble (Fig. 1b and d) occurs when Ω is around 3 whereas for an uncoated bubble it is expected to occur when Ω is equal to 2 (Eller et al. 1969).

To better compare the fundamental and subharmonic "resonance frequencies" of the bubbles at various acoustic pressures, the frequency of maximum response was plotted as a function of the acoustic pressure in Figure 2 for three bubble sizes (2, 4 and 6 μm diameter). As before, the shell parameters were: $\sigma(R_0) = 0$, $\chi = 2.50$ N/m and $\kappa_s(R_0)$.

As explained before in Figure 1a, the 2 μm diameter bubble indicates no local maximum in the fundamental response due to overdamping. However, the peak of the subharmonic resonance curve slightly shifts toward higher frequencies from 4.10 MHz at 1 kPa to 4.50 MHz at 120 kPa. For the other two bubbles, the fundamental and subharmonic responses follow a different trend with increasing acoustic pressure. The fundamental resonance frequency of the 4 μm bubble tends to decrease with increasing pressure while the subharmonic response behaves just the opposite. On the other hand, the fundamental and subharmonic resonance frequencies of the 6 μm diameter bubble seem to follow a different trend: a lower resonance frequency at higher acoustic pressure; the fundamental resonance frequency decreases almost 21% from 1.40 MHz to 1.10 MHz by increasing the pressure from 1 kPa to 120 kPa. The same happens for the subharmonic response, with the difference that the resonance frequency falls off less evidently (4%). This behavior is in agreement with the numerical and experimental results of Overvelde et al. (2010) for the resonance curves of a 6 μm diameter bubble derived from the oscillation amplitudes at the fundamental frequency.

EXPERIMENTS

Experimental set up

Figure 3 shows the schematic view of the set up. Highly diluted BR14 microbubbles (Bracco Research S.A., Geneva, Switzerland) were injected with a syringe inside a 200 μm diameter acoustically transparent cellulose capillary fiber with an 8 μm wall thickness (Product No. 132294; Spectrum Europe, Breda, The Netherlands) kept in a small water tank filled with Isoton II (Beckman Coulter, Woerden, The Netherlands). The capillary was located at the focal point of the transducer. A wide band transducer (V311; 3-13 MHz, Panametrics, Aarselaar, Belgium, or PA076; 1-9 MHz, Precision Acoustics, Dorchester, UK) was used for transmit. The transducer was connected to a power amplifier (150A100B; Amplifier Research, Limerick, Ireland), which amplified the wave generated by an arbitrary wave generator (8026; Tabor Electronics Ltd., Tel Hanan, Israel). Bursts of a 25-cycle sinusoidal wave, tapered with a Gaussian envelope at the first and last two cycles were transmitted. For the majority of small bubbles (diameter <3 μm), transmitted frequencies between 8–11 MHz with a frequency step of 200 kHz were chosen. Most of the larger bubbles were insonified in the frequency range of 4–7 MHz with frequency steps of 200 kHz. The pressure at focus for each experiment was changed from 50 kPa to 100 kPa and finally 120 kPa. These pressure values were calibrated using a 0.2 mm PVDF probe hydrophone (Precision Acoustics Ltd., Dorchester, UK). The relatively low pressures used ensured no changes in the bubble size after insonification.

The region-of-interest was illuminated with an optical light guide (SCHOTT AG, Mainz, Germany)

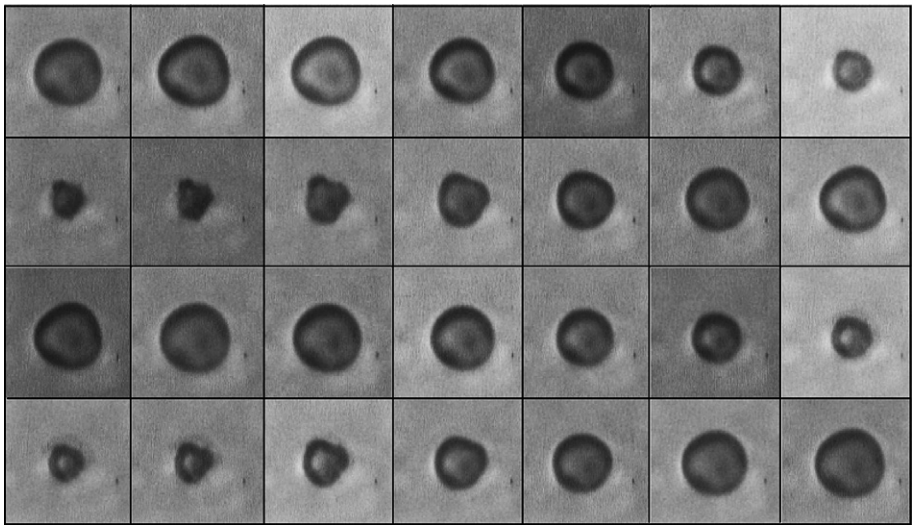

Fig. 4. Twenty-eight frames from the recording of a 4.60 μm bubble insonified at transmitting frequency of 4.20 MHz and acoustic pressure of 100 kPa.

connected to a Xenon flash lamp (A-260, Vision Light Tech, Uden, The Netherlands). An Olympus microscope with a $\times$60 water-immersed objective (NA = 0.9) was focused on the bubbles inside the capillary. The total magnification of the system was further increased to $\times$240 by using an additional 2 $\times$ 2 magnification lens inside the microscope. The radial response of the insonified bubble was recorded with an ultra-fast recording camera, the Brandaris 128, (Chin et al. 2003) at a frame rate of 20 million frames per second. The camera was set to record 49 movies of 128 frames in a single run. The first recording was always done without ultrasound to have an estimate of the resting radius of the bubbles and of the noise level of the system. In the subsequent movies, the frequency was swept in 16 steps in ascending order to cover the required frequency range at acoustic pressure of 50 kPa, followed by 16 frequency steps at 100 kPa and finally 16 frequency steps at 120 kPa. As an example, we display 28 frames from the recording of a 4.6 μm bubble insonified at transmitting frequency of 4.20 MHz and acoustic pressure of 100 kPa (Fig. 4). The frames show clearly the buckling of the shell during oscillations in this bubble. Each recording was stored in the computer for further analysis. From each individual movie, the diameter of the microbubble as a function of time (DT-curve) was measured using custom-designed image analysis software (Van der Meer et al. 2007). An edge detection algorithm based on a minimum-cost analysis (MCA) was used to trace the circumference of the bubbles. At the first frame, a circle is defined around the bubble. The center point of this contour is used to resample the bubbles and its direct surrounding using the gray-scale slope along the radial direction as the cost function. The algorithm finds the optimal path along the contour indicating the boundary of the bubble area. We define the diameter of the bubble as the diameter of a circle with an area equal to the detected boundary. This procedure is repeated for all the frames and, at the end, the diameter of the bubble is plotted vs. time producing a DT-curve. The Discrete Fourier transform of DT-curves was then calculated that gives the maximum amplitude of radial excursion at resonance of the bubble.

The ideal case would be to measure both the fundamental and subharmonic resonance curves of a bubble in a single experiment. For that purpose, one should sweep the driving frequency in a wide range going at least from half to three times the fundamental resonance frequency. At high frequencies applied here, there are, however, two unavoidable limiting factors: first, the bandwidth of the transmitting and receiving transducers mentioned above and, second, the sampling frequency of the ultra-high speed camera (21 MHz), which has to be at least twice the maximum driving frequency to avoid aliasing. Therefore, for each single bubble, we are here practically bound to measure either the fundamental or the subharmonic resonance curve.

RESULTS

The responses of 390 individual single bubbles were recorded and analyzed. Thirty bubbles in the frequency range of 4–7 MHz and 360 in the range of 8–12 MHz.

As a typical example, we display six DT-curves (out of the set of 16) of a 4.40 μm diameter bubble in Figure 5. The transmit frequency in these selected graphs increases from 4.40 MHz to 6.40 MHz The amplitude of the acoustic pressure was 50 kPa. The FFT of the first recording from each bubble, which was done without

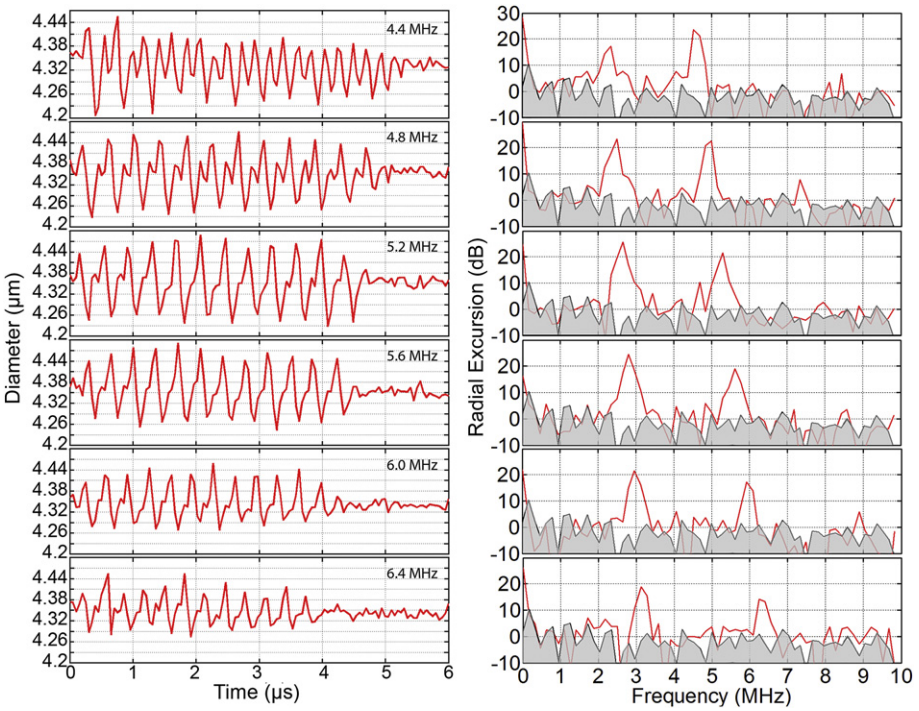

Fig. 5. Selected DT-curves (left panel) and corresponding power spectra (right panel) of a bubble with a diameter of 4.40 μm. Driving frequencies range between 4 to 7 MHz. The applied acoustic pressure is 50 kPa. The sampling time is 0.05 μs. The selection has been done between 4.40 MHz and 6.40 MHz with frequency step of 400 kHz. The gray area in the power spectra indicates the noise floor.

ultrasound, was used as the estimate of the noise level (gray area in Fig. 5). The corresponding power spectra show a peak at the fundamental driving frequency and at the subharmonic frequency (half the driving frequency). In this example, at a driving frequency of 5.20 MHz, the amplitude of subharmonic reaches a maximum at 2.70 MHz.

To study the dependence of the subharmonic amplitude as a function of the transmitted frequency, the amplitude of excursion at the subharmonic frequency was extracted from the DT-curves for all the recordings and plotted vs. frequency. The subharmonic resonance frequency was derived for each bubble by fitting the subharmonic resonance curves with a functional form displaying a single absolute maximum. We use for simplicity a Lorentzian function as follows (Leighton 1994):

$$\mathrm{Re}(f) = \frac{\mathrm{Re}_0}{\left(1-f^2/f_0^2\right)^2+(\delta f/f_0)^2} \qquad (7)$$

where f_0, δ and Re_0 are the fitting parameters.

The occurrence of the subharmonic

Figure 6 shows the size distribution of the recorded bubbles together with the size distribution of the bubbles showing subharmonic response. The median bubble diameter was 2.40 μm and the diameter ranged from 1 to 7 μm. Among the 30 measurements performed at frequency range between 4 and 7 MHz, one third showed a subharmonic response. For the rest of the bubbles which were insonified at 8–12 MHz, 40% indicated subharmonic oscillations. Although these bubbles had a diameter between 1.50 and 4.50 μm and the recorded bubble sizes are not equally distributed over the whole range, there are no indications that the amounts of bubbles that

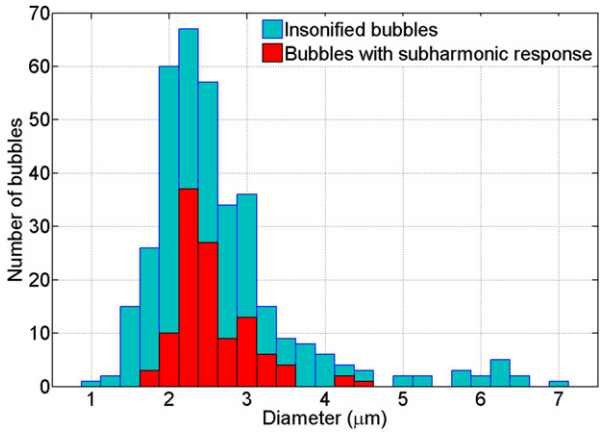

Fig. 6. Size distribution of investigated bubbles (blue bars) and those showing subharmonic response (red bars).

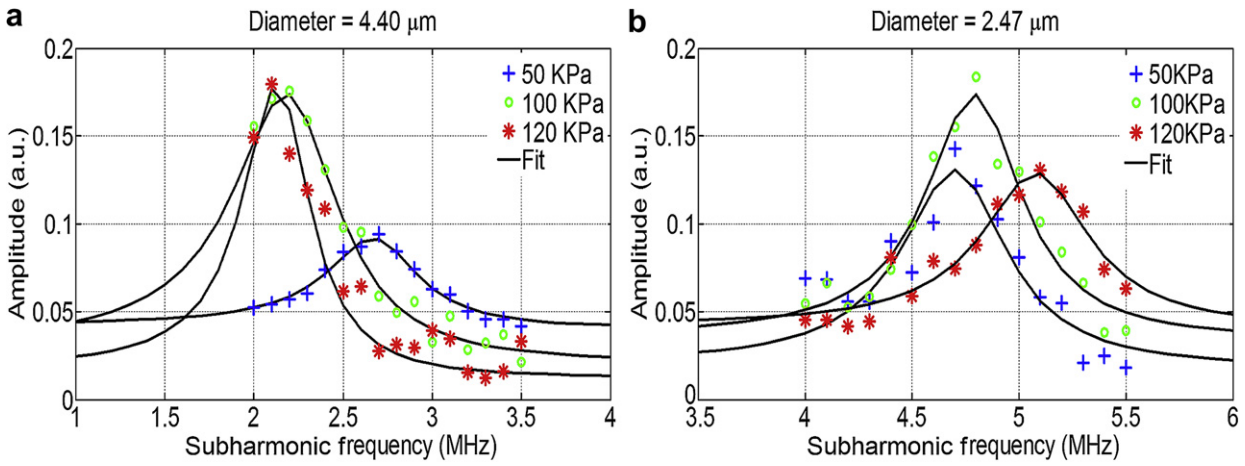

Fig. 7. The subharmonic amplitude as a function of the subharmonic frequency for (a) 4.40 μm and (b) 2.47 μm bubble at driving amplitude pressures of 50, 100 and 120 kPa. The fit on the experimental data was done using the Lorentzian function defined in eqn (7). Data on the abscissa have an uncertainty of ± 0.1 MHz.

show a subharmonic response are related to the bubble resting diameter.

The influence of the acoustic pressure on the subharmonic

Figure 7 shows the subharmonic resonance curves of two bubbles with a diameter of 4.40 μm and 2.47 μm insonified at a frequency of 4–7 MHz and 8–11 MHz, respectively. The first bubble (Fig. 7a) has a subharmonic resonance frequency of 2.70 MHz at 50 kPa, which decreases to 2.15 MHz at 120 kPa. The amplitude at the subharmonic resonance frequency increases for higher pressures. The smaller bubble (Fig. 7b) shows its maximum amplitude at the subharmonic resonance frequency of 4.70 MHz. The subharmonic frequency shifts to 5.10 MHz for higher pressures. In this case, the amplitude at the subharmonic resonance frequency first increases and then decreases. In general for relatively large bubbles investigated in the experiments (diameter > 3 μm), the subharmonic resonance frequency decreases with increasing driving pressure amplitude while it increases for smaller bubbles (diameter < 3 μm).

The influence of the bubble size on the subharmonic

Figure 8 shows the subharmonic resonance frequency of the bubbles vs. their diameter. Binning was performed over 100 nm. The bubble diameter varied between 1.40 μm and 4.40 μm. In the left panel, the results are plotted for an acoustic pressure of 50 kPa and, in the left panel. for 100 kPa.

For comparison, the fundamental resonance frequencies of an uncoated bubble (dash dotted line)

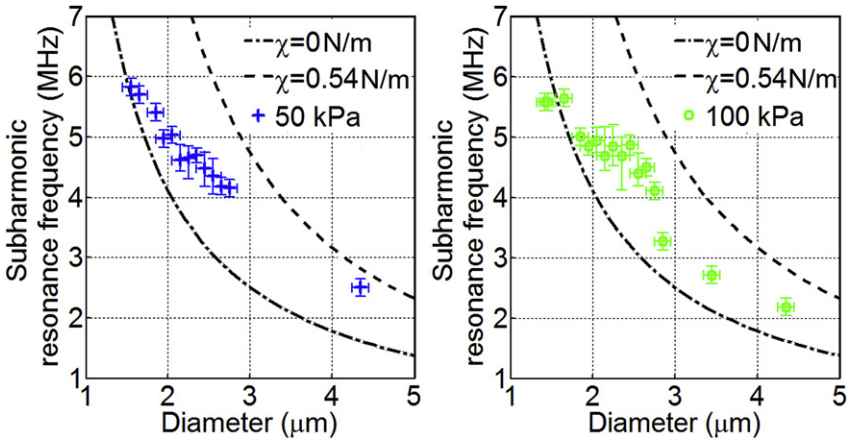

Fig. 8. Measured subharmonic resonance frequencies vs. diameter for two applied pressure of 50 kPa and 100 kPa after binning over 100 nm. Theoretical resonance frequencies obtained with eqn (4) for $\sigma(R_0) = \sigma_w$, $\chi = 0.54$ (dash line) and $\chi = 0$ (dash-dot line).

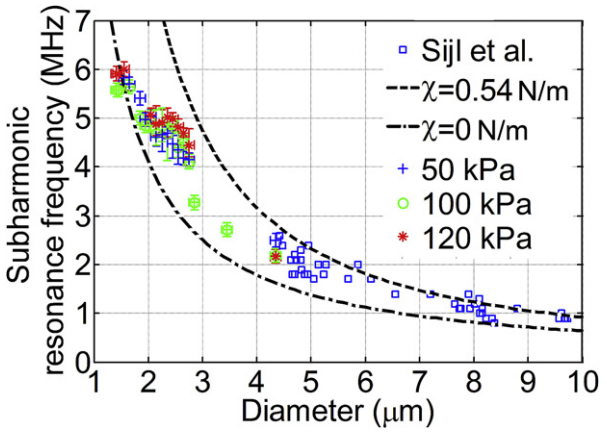

Fig. 9. Subharmonic resonance frequency vs. diameter of BR14 microbubbles. Dashed line is the fundamental resonance frequency predicted by the linearized viscoelastic model for $\chi = 0.54$ N/m and the dash-dotted line corresponds to $\chi = 0$ N/m.

and a linear viscoelastic bubble (dashed line) were also calculated using eqn (4). The effective value for shell elasticity $\chi = 0.54$ N/m is the value determined by Van der Meer et al. (2007) using eqn (4).

Our data set contains predominantly smaller bubbles as shown in Figure 6. To cover a larger range of microbubble size, we added 93 measurements that were performed at larger bubble range at acoustic pressure level of 100 kPa and described by Sijl et al. (2010). Figure 9 shows now the subharmonic resonance frequency for all the bubbles together with the predictions of the viscoelastic model. It can be concluded that the viscoelastic model matches very well with the experimental values of a bubble diameter larger than 5 μm but the prediction clearly fails for smaller bubbles.

DISCUSSION

The subharmonic behavior of a lipid coated contrast agent was investigated in the favored frequency range for carotid imaging (4–12 MHz). Forty percent of the investigated BR14 bubbles showed subharmonic oscillations (Fig. 6) and all of them vibrated with asymmetrical amplitude and by that showing the so called compression-only behavior. The fact that at low acoustic pressures the lipid coating induces highly nonlinear behavior, *e.g.*, compression-only, has been observed before (de Jong et al. 2007) and is also well described by Marmottant et al. (2005) model. It is likely that the reason for the absence of the subharmonics in the remainder 60% of studied bubbles is due to the difference in the concentration of the shell lipids. This difference in the framework of the Marmottant model corresponds to having different values of the surface tension at rest for bubbles of the same size. The value of $\sigma(R_0)$ fixes also the value of the

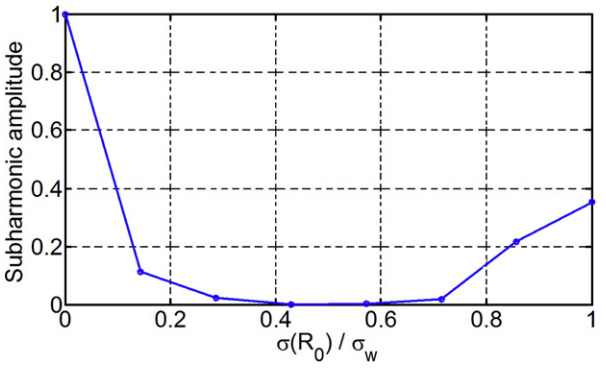

Fig. 10. Amplitude of subharmonic vs. the surface tension at rest of a 2.40 μm diameter bubble. The value of $\sigma(R_0)$ in the x-axis is normalized by σ_w. The amplitude of subharmonic in the y-axis is normalized by the amplitude of subharmonic at $\sigma(R_0) = 0$.

so called buckling radius R_b, *i.e.*, the radius below which the phospholipid elastic coating does not exert any tensional effect. The case $\sigma(R_0) = 0$ in particular implies $R_b = R_0$, meaning compressive bubble oscillations (compression-only) are strongly favored in this case since the surface tension is totally absent for $R < R_0 = R_b$; while it increases quadratically with R for $R > R_0$ [see eqn (2)]. As it has been shown in the study by Sijl et al. (2010), a compression-only behavior is associated with the presence of subharmonic resonances even at very low (5 kPa) driving pressures. When instead $\sigma(R_0) > 0$, one has $R_b < R_0$. In this case, buckling conditions are reached at higher driving pressures and, therefore, subharmonic resonance occurs less.

This hypothesis is also supported by our numerical simulations in which we have derived the amplitude of subharmonic as a function of $\sigma(R_0)$. Figure 10 displays the dependence of the subharmonic amplitude on the surface tension of a 2.40 μm diameter bubble. The value of $\sigma(R_0)$ is varied from 0 to σ_w and normalized by the surface tension of water. The amplitude of resonance is normalized by the amplitude of subharmonic at $\sigma(R_0) = 0$. The other shell parameters are kept the same as the previous simulations (Fig. 2). This result is also in very good agreement with the parametric study conducted by Sijl et al. (2010) for a 7.60 μm diameter bubble at driving pressure amplitude and frequency of 40 kPa and 2.40 MHz. The highest subharmonic response is observed when the surface tension of a coated bubble at rest is zero. A slight increase in the value of $\sigma(R_0)$ results in a dramatic decrease in the subharmonic amplitude in which at $\sigma(R_0) = 0.04$ N/m no subharmonic response is detected. The output of these simulations all together shows the sensitivity of bubble dynamics to shell parameters. A little change in the resting surface tension results in a completely different behavior for the bubbles even with the same size (see also Frinking et al. 2010).

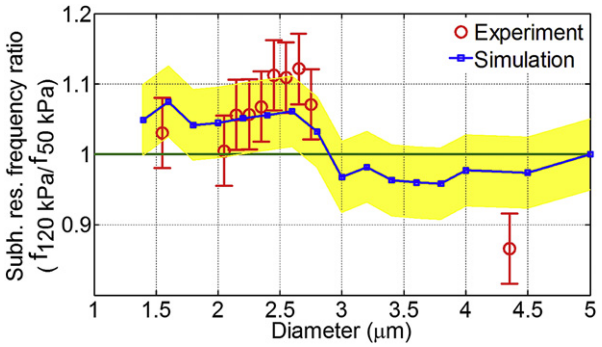

Fig. 11. Subharmonic resonance frequency ratio of 120 kPa and 50 kPa acoustic pressures vs. bubble diameter derived from experiment (circles) and simulation (squares). The filled area indicates the level of uncertainty in the simulations.

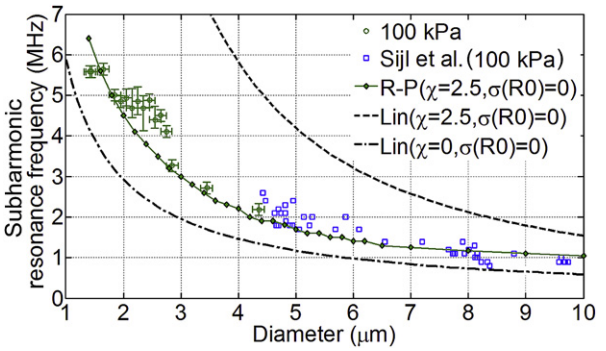

Fig. 12. comparison between linearized Rayleigh- Plesset (Lin) [eqn (4)] at two values of shell elasticity (0 and 2.50 N/m) and $\sigma(R_0) = 0$, the modified Rayleigh- Plesset (R-P)[eqn (1)] and the experimental measurements at acoustic pressure amplitude of 100 kPa.

Second, we observed a size dependent behavior for the subharmonic resonance frequency of microbubbles with the increase of acoustic pressure. Extracting the resonance curves of bubbles with subharmonic spectroscopy vs. applied acoustic pressure specifies two different regimes; bigger bubbles (>3 μm diameter) showed a decrease in the subharmonic resonance frequency for increasing the pressure; whereas for smaller bubbles (≤3 μm diameter), the subharmonic resonance frequency increases for increasing the pressure (Fig. 6). This phenomenon has not been observed for the fundamental resonance frequency. Overvelde et al. (2010) showed that the fundamental resonance frequency decreases for increasing acoustic pressure for all bubble sizes. This is confirmed by the simulations using the Marmottant model as shown in Figure 2.

The subharmonic resonance and its dependency on the acoustic pressure, however, is also predicted correctly by the Marmottant model as shown in Figure 11 using as shell parameters: $\sigma(R_0) = 0$, $\chi = 2.50$ N/m and $\kappa_s(R_0)$ adopted from Van der Meer et al. (2007). In the same figure, we also plot the ratio of the subharmonic resonance frequencies at 50 kPa and at 120 kPa vs. bubble diameter as derived from the measurements. The graph shows up to 10% increase in the resonance frequency of bubbles smaller than 3 μm in diameter by increasing the pressure from 50 kPa to 120 kPa. For larger bubbles, less experimental data are available. Nevertheless, opposite to what was explained before, the subharmonic frequency ratio decreases. This is qualitatively supported also by numerical simulations.

The explained behavior for small bubbles (≤3 μm diameter) is a phenomenon known as shell (strain) hardening in contrast to bigger bubbles (>3 μm diameter), which show shell softening for the acoustic pressure increase. Shell (strain) softening is a rheologic effect, which indicates the decrease in the shell elasticity of a material as the deformation strength increases (Doinikov et al. 2009). The comparison between these two regimes once again asserts the choice of zero surface tension at rest for the small bubbles.

We also compared the results of the experiments with the predictions of the linearized viscoelastic model using the value for shell elasticity ($\chi = 0.54$ N/m) reported by Van der Meer et al. (2007). This value was found with the assumption of a linearized viscoelastic model on the fundamental resonance frequency of bubbles. Using this value delivered disappointing results for small bubbles although it has a good agreement for bigger bubbles (Fig. 9).

One important feature neglected in the derivation of the linearized viscoelastic model is the dynamic surface tension [eqn (2)], which varies for different bubble sizes. Another size-dependent shell parameter is the shell viscosity. Van der Meer et al. (2007) have shown that κ_s decreases for increasing dilatation rate, corresponding to a shear-thinning behavior. Pseudoplastic or shear-thinning fluids have a lower apparent viscosity at higher shear rates, and are usually solutions of large, polymeric molecules in a solvent with smaller molecules (Schowalter 1978; Macosko 1994). It is generally supposed that the large molecular chains tumble at random and affect large volumes of fluid under low shear but they gradually align themselves in the direction of increasing shear and produce less resistance. By taking all these points into consideration, inserting the shell parameters: $\sigma(R_0) = 0$, $\chi = 2.50$ N/m and $\kappa_s(R_0)$ as derived by Van der Meer et al. into the Marmottant et al. model presents an excellent agreement with the experiment as shown in Figure 12.

Finally, it was shown that the frequency of the subharmonic response of coated bubbles is not locked to the frequency of the fundamental resonance; instead, their respective ratio depends on the applied acoustic pressure (Fig. 2). Therefore, it is not accurate to assume that the

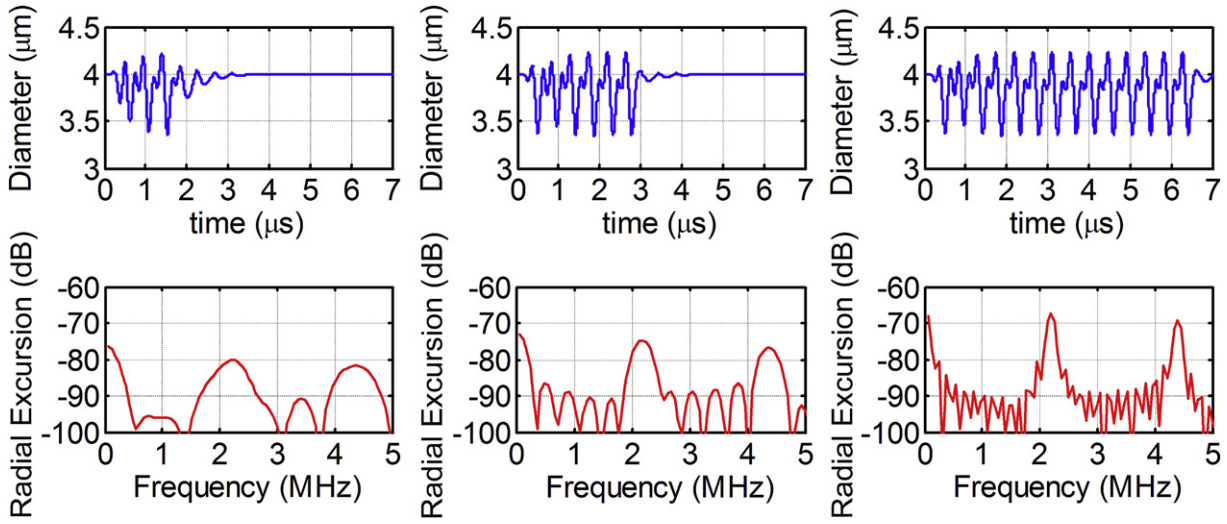

Fig. 13. Response of a 4 μm diameter bubble to a pressure pulse with the amplitude of 120 kPa at the transmitting frequency of 4.40 MHz. The length of the burst (from left to the right) has increased from five cycles to 10 and 25, respectively. DT-curves are shown in the upper panels and the lower panels present the corresponding power spectra.

highest value of subharmonic amplitude occurs always at the double frequency of the fundamental resonance frequency of a microbubble. Depending on the size and shell parameters, this factor can vary from one bubble to the other. For example, the 4 μm diameter bubble reported in Figure 2, has the subharmonic resonance frequency of 2.10 MHz at 1 kPa. This means that the transmitting frequency in which the subharmonic resonance frequency was derived was 4.20 MHz. The ratio between this value and the fundamental resonance frequency of the bubble at the same pressure (which is also reported in the same figure as 2.40 MHz) is 1.70. The same calculation at 120 kPa gives a ratio equal to 2.40. Therefore, for a 4 μm diameter bubble with a resting surface tension of zero, this factor varies between 1.70 and 2.40 at different acoustic pressures.

As already mentioned at the end of the "Experimental set up" section, at present, the simultaneous comparison of the fundamental and subharmonic responses of a bubble is not experimentally feasible. Therefore, we had to limit the analysis to the comparison of the experimental results with the outcomes of the simulations. This highlights the importance of a predictive model explaining the behavior typical for bubble sizes <3 μm and careful choice of shell parameters.

The results derived from this study provide the basic knowledge for using the subharmonic response of ultrasound contrast agents in carotid imaging. For clinical applications, normal pulse lengths shorter than the 25-cycle bursts applied in our experiments are used. Nevertheless, we show in the following (Fig. 13) that the same can be achieved by implementing a shorter pulse, which is more relevant for clinical scanners. The results of numerical simulations, presented in Figure 13, show the response of a 4 μm diameter bubble to the pressure pulse described previously (see numerical model section) with the amplitude of 120 kPa at the insonifying frequency of 4.40 MHz. The length of the burst has increased from five cycles to 10 and 25, respectively. As can be seen in the figures, the subharmonic energy is already present in the first cycles and its level compared with the fundamental response remains equal.

Furthermore, to adapt the existing clinical scanners for subharmonic carotid imaging, it is crucial to characterize the subharmonic oscillation of contrast agent microbubbles also acoustically, which is what a scanner would actually measure. An acoustical study on the subharmonic response of these microbubbles, complementary to the optical study presented here, will be reported in a forthcoming article.

CONCLUSION

For the frequencies between 4 and 12 MHz, 40% of the bubbles exhibited a subharmonic response. These bubbles had a diameter between 1 and 4 μm. The subharmonic resonance frequency for bubbles smaller than 3 μm is not the same as the fundamental resonance frequency. Furthermore, the subharmonic resonance frequency of this bubble size increased up to 10% with increasing acoustic pressure from 50 to 120 kPa. This observation indicates a shell hardening effect, just the opposite of what was observed for the fundamental response.

The proper choice of shell parameters: $\sigma(R_0) = 0$, $\chi = 2.50$ N/m and $\kappa_s(R_0)$ presenting shear thinning

resulted in an excellent agreement between the Marmottant model and the experimental data.

Acknowledgments—The authors would like to thank Frits Mastik for his support on Brandaris recordings and Benjamin Dollet, Guillaume Renaud and Enrico Calzavarini for their valuable comments.

REFERENCES

Baldassarre D, Amato M, Bondioli A, Sirtori CR, Tremoli E. Carotid artery intima-media thickness measured by ultrasonography in normal clinical practice correlates well with atherosclerosis risk factors. Stroke 2000;31:2426–2430.

Barger AC, Beeuwkes R, Lainey LL, Silverman KJ. Hypothesis: *Vasa vasorum* and neovascularization of human coronary arteries. N Engl J Med 1984;310:175–177.

Biagi E, Breschi L, Vannacci E, Masotti L. Stable and transient subharmonic emissions from isolated contrast agent microbubbles. IEEE Trans Ultrason Ferroelectr Freq Control 2007;54:480–497.

Brock-Fisher GA, Poland MD, Rafter PG. 1996. Means for increasing sensitivity in non-linear ultrasound imaging systems. US Patent No. 5577505.

Burns PN, Wilson SR, Simpson DH. Pulse inversion imaging of liver blood flow: Improved method for characterizing focal masses with microbubble contrast. Invest Radiol 2000;35:58–71.

Chang PH, Shung KK, Wu S, Levene HB. Second harmonic imaging and harmonic Doppler measurements with Albunex. IEEE Trans Ultrason Ferroelectr Freq Control 1995;42:1020–1027.

Chin CT, Lancee C, Borsboom J, Mastik F, Frijlink M, de Jong N, Versluis M, Lohse D. Brandaris 128: A 25 million frames per second digital camera with 128 highly sensitive frames. Rev Sci Instrum 2003;74:5026–5034.

Chomas J, Dayton P, May D, Ferrara K. Nondestructive subharmonic imaging. IEEE Trans Ultrason Ferroelectr Freq Control 2002;49: 883–892.

Church CC. The effects of an elastic solid surface layer on the radial pulsations of gas bubbles. J Acoust Soc Am 1995;97:1510–1521.

Coli S, Magnoni M, Sangiorgi G, Marrocco-Trischitta MM, Melisurgo G, Mauriello A, Spagnoli L, Chiesa R, Cianflone D, Maseri A. Contrast-enhanced ultrasound imaging of intraplaque neovascularization in carotid arteries: Correlation with histology and plaque echogenicity. J Am Coll Cardiol 2008;52:223–230.

de Jong N, Emmer M, Chin CT, Bouakaz A, Mastik F, Lohse D, Versluis M. Compression-only behavior of phospholipid-coated contrast bubbles. Ultrasound Med Biol 2007;33:653–656.

de Jong N, Hoff L. Ultrasound scattering properties of Albunex microspheres. Ultrasonics 1993;31:175–181.

de Santis P, Sette D, Wanderlingh F. Cavitation detection: The use of the subharmonics. J Acoust Soc Am 1967;42:514–516.

Doinikov AA, Haac JF, Dayton PA. Modeling of nonlinear viscous stress in encapsulating shells of lipid-coated contrast agent microbubbles. Ultrasonics 2009;49:269–275.

Eliasziw M, Rankin RN, Fox AJ, Haynes RB, Barnett HJM. Accuracy and prognostic consequences of ultrasonography in identifying severe carotid artery stenosis. Stroke 1995;26:1747–1752.

Eller HGF. Generation of subharmonics of order one-half by bubbles in a sound field. J Acoust Soc Am 1969;46:722–727.

Feinstein SB. Atherosclerotic plaque neovascularization contrast ultrasound imaging of the carotid artery *vasa vasorum* and atherosclerotic plaque neovascularization. J Am Coll Cardiol 2006;48: 236–243.

Frinking P, Cespedes EI, Kirkhorn J, Torp HG, de Jong N. A new ultrasound contrast imaging approach based on the combination of multiple imaging pulses and a separate release burst. Int Ultrason Symp Proc 2001;48:643–651.

Frinking P, Gaud E, Arditi M. Compression-only behavior and subharmonic scattering of phospholipid-shell microbubbles. IEEE Int Ultrason Symp Proc 2009;978:4244–4390.

Frinking PJA, Gaud E, Brochot J, Arditi M. Subharmonic scattering of phospholipid-shell microbubbles at low acoustic pressure amplitudes. IEEE Trans Ultrason Ferroelectr Freq Control 2010;57: 1762–1771.

Goertz DE, Cherin E, Needles A, Karshafian R, Brown AS, Burns PN, Foster FS. High frequency nonlinear B-scan imaging of microbubble contrast agents. IEEE Trans Ultrason Ferroelectr Freq Control 2005; 52:65–79.

Goertz DE, Frijlink ME, Tempel D, Bhagwandas V, Gisolf A, Krams R, de Jong N, van der Steen AFW. Subharmonic contrast intravascular ultrasound for *vasa vasorum* Imaging. Ultrasound Med Biol 2007; 33:1859–1872.

Golledge J, Greenhalgh RM, Davies AH. The symptomatic carotid plaque. Stroke 2000;31:774–781.

Gössl M, Rosol M, Malyar NM, Fitzpatrick LA, Beighley PE, Zamir M, Ritman EL. Functional anatomy and hemodynamic characteristics of *vasa vasorum* in the walls of porcine coronary arteries. Anat Rec A 2003;272A:526–537.

Hoff L, Sontum P, Hovem J. Oscillations of polymeric microbubbles: Effect of the encapsulating shell. J Acoust Soc Am 2000;107: 2272–2280.

Keller JB, Miksis MJ. Bubble oscillations of large amplitude. J Acoust Soc Am 1980;68:628–633.

Krishna PD, Shankar PM, Newhouse VL. Subharmonic generation from ultrasonic contrast agents. Phys Med Biol 1999;44:681–694.

Lauterborn W. Numerical investigation of nonlinear oscillations of gas bubbles in liquids. J Acoust Soc Am 1976;59:283–293.

Leighton TG. The acoustic bubble. London: Academic Press Limited; 1994.

Lotsberg O, Hovem JM, Aksum B. Experimental observation of subharmonic oscillations in infoson bubbles. J Acoust Soc Am 1996;99: 1366–1369.

Macosko CW. Rheology Principles, Measurements and Applications. Wiley-VCH; 1994.

Marmottant P, Van der Meer S, Emmer M, Versluis M, de Jong N, Hilgenfeldt S, Lohse D. A model for large amplitude oscillations of coated bubbles accounting for buckling and rupture. J Acoust Soc Am 2005;118:3499–3505.

Mause SF, Weber C. Intrusion through the fragile back door immature plaque microvessels as entry portals for leukocytes and erythrocytes in atherosclerosis. J Am Coll Cardiol 2009;53:1528–1531.

Minnaert M. On musical air bubbles and the sound of running water. Philos Mag 1933;16:235–248.

Needles A, Arditi M, Rognin NG, Mehi J, Coulthard T, Bilan-Tracey C, Gaud E, Frinking P, Hirson D, Foster FS. Nonlinear contrast imaging with an array based micro-ultrasound system. Ultrasound Med Biol 2010;36:2097–2106.

Neppiras EA. Subharmonic and other low-frequency emission from bubbles in sound-irradiated liquids. J Acoust Soc Am 1969;46: 587–601.

Overvelde M, Garbin V, Sijl J, Dollet B, De Jong N, Lohse D, Versluis M. Nonlinear shell behavior of phospholipid-coated microbubbles. Ultrasound Med Biol 2010;36:2080–2092.

Plesset MS. The dynamics of cavitation bubbles. J Appl Mech 1949;16: 277–282.

Plesset MS, Prosperetti A. Bubble dynamics and cavitation. Ann Rev Fluid Mech 1977;9:145–185.

Prosperetti A. Nonlinear oscillations of gas bubbles in liquids: Steady state solutions. J Acoust Soc Am 1974;56:878–885.

Prosperetti A. Nonlinear oscillations of gas bubbles in liquids. Transient solutions and the connection between subharmonic signal and cavitation. J Acoust Soc Am 1975;57:810–821.

Prosperetti A. Application of the subharmonic threshold to the measurement of the damping of oscillating gas bubbles. J Acoust Soc Am 1977;61:11–16.

Ritman EL, Lerman A. The dynamic *vasa vasorum*. Cardiovasc Res 2007;75:649–658.

Schaar JA, Muller JE, Falk E, Virmani R, Fuster V, Serruys PW, Colombo A, Stefanadis C, Ward Casscells S, Moreno PR, Maseri A, van der Steen AF. Terminology for high-risk and vulnerable coronary artery plaques. Eur Heart J 2004;25:1077–1082.

Schowalter WR. Mechanics of non-Newtonian fluids. Oxford-Frankfurt: Pergamon Press; 1978.

Shah F, Balan P, Weinberg M, Reddy V, Neems R, Feinstein M, Dainauskas J, Meyer P, Goldin M, Feinstein SB. Contrast-enhanced ultrasound imaging of atherosclerotic carotid plaque neovascularization: A new surrogate marker of atherosclerosis? Vasc Med 2007;12:291–297.

Shalhoub J, Owen DRJ, Gauthier T, Monaco C, Leen ELS, Davies AH. The use of contrast enhanced ultrasound in carotid arterial disease. Eur J Vasc Endovasc Surg 2010;39:381–387.

Shankar PM, Krishna PD, Newhouse VL. Advantages of subharmonic over second harmonic backscatter for contrast-to-tissue echo enhancement. Ultrasound Med Biol 1998;24:395–399.

Shankar PM, Krishna PD, Newhouse VL. Subharmonic backscattering from ultrasound contrast agents. J Acoust Soc Am 1999;106: 2104–2110.

Shi WT, Forsberg F, Hall AL, Chiao RY, Liu JB, Miller S, Thomenius KE, Wheatley MA, Goldberg BB. Subharmonic imaging with microbubble contrast agents: Initial results. Ultrason Imaging 1999;21:79–94.

Sijl J, Dollet B, Overvelde M, Garbin V, Rozendal T, De Jong N, Lohse D, Versluis M. Subharmonic behavior of phospholipid-coated ultrasound contrast agent microbubbles. J Acoust Soc Am 2010;128:3239–3252.

Sluimer JC, Daemen MJ. Novel concepts in atherogenesis: Angiogenesis and hypoxia in atherosclerosis. J Pathol 2009;218:7–29.

Staub D, Patel MB, Tibrewala A, Ludden D, Johnson M, Espinosa P, Coll B, Jaeger KA, Feinstein SB. *Vasa vasorum* and plaque neovascularization on contrast-enhanced carotid ultrasound imaging correlates with cardiovascular disease and past cardiovascular events. Stroke 2009;41:41–47.

Van der Meer SM, Dollet B, Voormolen MM, Chin CT, Bouakaz A, de Jong N, Versluis M, Lohse D. Microbubble spectroscopy of ultrasound contrast agents. J Acoust Soc Am 2007;121:648–656.

Vicenzini E, Giannoni MF, Puccinelli F, Ricciardi MC, Altieri M, Di Piero V, Gossetti B, Benedetti Valentini F, Lenzi GL. Detection of carotid adventitial *vasa vasorum* and plaque vascularization with ultrasound cadence contrast pulse sequencing technique and echocontrast agent. Stroke 2007;38:2841–2843.

Virmani R, Kolodgie FD, Burke AP, Farb A, Schwartz SM. Lessons from sudden coronary death: A comprehensive morphological classification scheme for atherosclerotic lesions. Arterioscler Thromb Vasc Biol 2000;20:1262–1275.

Xiong L, Deng YB, Zhu Y, Liu YN. Correlation of carotid plaque neovascularization detected by using contrast-enhanced US with clinical symptoms. Radiology 2009;251:583–589.

Yach D, Hawkes C, Gould CL, Hofman KJ. The global burden of chronic diseases– Overcoming impediments to prevention and control. JAMA 2004;291:2616–2622.

Zamir M, Silver MD. Vasculature in the walls of human coronary arteries. Arch Pathol Lab Med 1985;109:659–662.